Theoretical study of the enhancement of saturable absorption of Kr under x-ray free-electron laser

Jiaxin Ye(叶佳鑫)[1,2], Yixuan Yang(杨怡璇)[3], Chen Yang(杨晨)[1,2,†], and Gang Jiang(蒋刚)[1,2,‡]

[1] *Institute of Atomic and Molecular Physics, Sichuan University, Chengdu* 610065, *China*
[2] *Key Laboratory of High Energy Density Physics and Technology, Ministry of Education, Chengdu* 610065, *China*
[3] *College of Electrical Engineering, Sichuan University, Chengdu* 610065, *China*

(Received 20 May 2022; revised manuscript received 2 August 2022; accepted manuscript online 26 August 2022)

The generation of hollow atoms will reduce the probability of light absorption and provide a high-quality diffraction image in the experiment. In this paper, we calculated the ionization rate of the Kr atom under x-ray free-electron laser (XFEL) using Hartree–Fock–Slater model and simulated the ionization model of Kr atom using Monte–Carlo method to determine the response of the hollow atom of Kr atom to the XFEL photon energy. Calculating the correlation between the total photoionization cross-section of the ground state of Kr atom and the photon energy, we determined three particular photon energies of 1.75 keV, 1.90 keV, and 14.30 keV. The dynamics simulation under the experimental condition's 17.50 keV photon energy was achieved by implementing the Monte–Carlo method and calibrating the photon flux modeling parameters. Consequently, our calculated data are more consistent with experimental phenomena than previous theoretical studies. The saturable absorption of Kr at 1.75 keV, 1.90 keV, 14.30 keV, and 17.50 keV energies was further investigated by using the optimized photon flux model theory. We compared the statistics on main ionization paths under those four specific photon energies and calculated the population changes of various Kr hollow atoms with different configurations. The results demonstrate that the population of hollow atoms produced at the critical ionization photon energy is high. Furthermore, the change of population with respect to position is smooth, which shows a significant difference between the generation mode of ions with low and high photon energies. The result is important for the study of medium- and high-Z element hollow atoms, which has substantial implications for the study of hollow atoms with medium and high charge states, as well as for the scaling of photon energy of free electron lasers.

Keywords: x-ray free-electron lasers, krypton, hollow atoms, Monte–Carlo simulation

PACS: 32.80.Hd, 32.80.Aa **DOI:** 10.1088/1674-1056/ac8cdd

1. Introduction

X-ray free-electron laser (XFEL) is known as the fourth-generation light source.[1] XFEL opens up new opportunities in exploring substances at the atomic and molecular scales of space and time, photographing chemical processes within a few milliseconds or less, and revealing the structure and dynamics of complex molecular systems.[2,3] In recent years, free-electron laser measurements of protein structures have become an increasingly valuable tool in biology.[4,5] At the same time, coherent x-ray diffraction imaging provides images of small structures, which is a major focus of crystallography and protein research.[6] It is of great significance to investigate the dynamical evolution of atoms under a laser to assess the radiation damage phenomenon in sample structure detection by using free-electron lasers.[7–9]

In experiments, x-ray photoionization can produce light transparency in aluminum.[10] When an atom interacts with the XFEL, the inner electrons are ionized, resulting in saturable absorption. This phenomenon reduces the probability of light-induced damage. In addition, the diffraction image obtained achieves the best quality.[11–14] According to the European XFEL, the range of photon energy that can be achieved during the current experiment is 0.2–25 keV.[15,16] Due to the limitation of photon energy generated by a laser and the hollow atoms in medium- and high-Z elements have high decay probability, the saturable absorption is not apparent. Thus, research on medium- and high-Z element hollow atoms is relatively scarce. Nevertheless, considering the photon energy is close to the ionization energy, when the ionization energy increases and exceeds the photon energy after the inner electron is ionized, it is possible to make the saturable absorption evident and durable, which makes the practical application of hollow atoms in the characterization of material structure possible.

The photon energy close to the orbital energy is called critical ionization photon energy (CIPE). Consequently, we extend the study of hollow atoms to Kr and examine the phenomenon of hollow atoms at photon energies close to their orbital energies. In this work, we implemented a genetic algorithm (GA) to determine laser parameters in the model and simulate the dynamical evolution of the Kr atom under three CIPEs by theoretical calculation.

[†]Corresponding author. E-mail: yangchen@scu.edu.cn
[‡]Corresponding author. E-mail: gjiang@scu.edu.cn

© 2023 Chinese Physical Society and IOP Publishing Ltd

2. Theoretical method

2.1. Theoretical model

Our calculation of the photoionization cross-section is based on the *ab initio* calculation framework of non-relativistic quantum electrodynamics and perturbation theory, using the Hartree–Fock–Slater (HFS) model.[18] The cross-section for photoionization of an electron in the ith occupied spin orbital follows

$$\sigma_i = \frac{4\pi^2}{\omega_{\rm in}}\alpha\sum_f \left|\left\langle \varphi_f \left| \mathrm{e}^{\mathrm{i}\boldsymbol{k}_{\rm in}\cdot\boldsymbol{x}}\varepsilon_{\boldsymbol{k}_{\rm in},\lambda_{\rm in}}\cdot\frac{\nabla}{\mathrm{i}}\right|\varphi_i\right\rangle\right|^2 \times\delta\left(\varepsilon_f-\varepsilon_i-\omega_{\rm in}\right), \tag{1}$$

where $\omega_{\rm in}$ is the incident photon energy, α is the fine structure constant, $\boldsymbol{x}$ is the position, $\varepsilon_{\boldsymbol{k}_{\rm in},\lambda_{\rm in}}$ is the polarization vector under the wave vector $\boldsymbol{k}$ and wavelength λ, ε_f is the energy of unoccupied orbital, ε_i is the energy of occupied orbital, φ_f is the sum of unoccupied orbital wave functions, and φ_i is the sum of occupied orbital wave functions.

We evaluated the ionization data of non-relativistic HFS model and relativistic Dirac–Fock–Slater (DFS) model, respectively. The selection difference of CIPEs is 3.71%, the ionization data difference range between the two models is 1.71%–9.29%, and the average data of ionization data difference is 4.58%. The most significant differences in ionization data occur in the highly ionized states of the atoms. As this study's Kr atom ionization model does not include ionized states (up to Kr^{10+}), a relativistic effect is not evident. In the study of the interactions between free electron lasers and atoms, the HFS model has been widely used and proven to be efficient.[19–21]

2.2. Photon flux modeling

Since the calculation of photoionization probability depends on photon flux, the modeling of photon flux is crucial for us to fit the theoretical calculation results. In the actual experiment of free-electron laser, the distribution of light intensity follows not only the Gaussian distribution of time, but also the Gaussian distribution of position and photon frequency. We assume that the beam is a circular spot, and the general formula of light intensity satisfies the Gaussian distribution of space, time, and photon frequency,[19–21]

$$I_\nu(r,t) = I_0\,\mathrm{e}^{-\ln 2a\left(\frac{r_1}{\Delta}\right)^2}\mathrm{e}^{-\ln 2\left(\frac{t}{T}\right)^2}\sqrt{\frac{\ln 2}{\pi\Gamma^2}}\,\mathrm{e}^{-\ln 2\left(\frac{h\nu-h\nu_0}{\Gamma}\right)^2}. \tag{2}$$

For convenience, we define the relative radius position r as

$$r = \frac{r_1}{\Delta}, \tag{3}$$

where t is the time, r_1 is the relative center position, ν is the photon frequency, Δ is the radius, τ is the pulse half-width, Γ is the half-width at the half-maximum (HWHM) of the photon frequency bandwidth, and $h\nu_0$ is the central photon energy. The exponential coefficient a and the peak flux I_0 are the laser parameters to be calibrated. The photoionization rate can be obtained by integrating the photon frequency bandwidth

$$R_{ij}(r,t) = \int \frac{I_\nu(r,t)}{h\nu}\sigma_{ij}(h\nu)\mathrm{d}\nu. \tag{4}$$

We can get the function of the photoionization rate by integrating the photon frequency. The energy of the x-ray pulse can be obtained by integrating the intensity of space, time, and photon energy. We used a genetic algorithm to calibrate the peak flux and exponential coefficient of Kr atom at 17.50 keV photon energy. Our calibrated parameters for the peak flux is 1.6×10^{12} photons/μm^2, and the index coefficient is 1.85. Benefit from the calibration of the parameters by the genetic algorithm, a series of calculations of 1.75 keV, 1.90 keV, and 14.30 keV make our theoretical calculation results more reliable.

2.3. Numerical method

The transition between electronic configurations can be well described by establishing the relevant rate equation between configurations. The equation form is as follows:

$$\frac{\mathrm{d}n_i}{\mathrm{d}t} = \sum_{j\neq i}^{N} n_j R_{ji} - n_i\sum_{j\neq i}^{N} R_{ij}. \tag{5}$$

When solving the ionization dynamics of Kr atom at each photon energy, we use the Monte–Carlo method, where R_{ij} is the rate from state i to state j, and n_i is the ratio of the total number of events at energy level i to the total number of events N. The total value of events depends on the parameters set by the Monte–Carlo method. This method is often used to solve the ionization dynamics of atoms. It can give a better evolutionary relationship of atomic ion population from massive data. Moreover, when the electron number increases, the Monte–Carlo method has been proved to be one of the most practical methods in atomic and molecular physics and materials science.[22–25] We used the XATOM toolkit[14] to calculate the photoionization cross-section, Auger decay, and fluorescence decay of atoms. We calculated the photoionization cross-section, Auger rate, and fluorescence rate of Kr at 1.75 keV, 1.90 keV, 14.30 keV, and 17.50 keV[26,27] by using our own Monte–Carlo program. In addition, our Monte–Carlo calculation details are as follows.

1. Read the electronic configuration as the key, and read the ionization, Auger and fluorescence decay rates of Kr atoms as the key values (the configuration only inputs the number of electrons in each shell) and give the initial time $t = 0$, and then select the photon flux at different positions.

2. Determine the appropriate time interval Δt and calculate the probability of photoionization, Auger decay, and fluorescence decay for electronic configuration (there are 82 possible channels for Kr). The probability (P_k) calculation formula

can be given as follows:

$$\begin{cases} P_{k1} = R_{ij} \cdot \Delta t & \text{for photoionization,} \\ P_{k2} = \Gamma_{ij}^{\mathrm{A}} \cdot \Delta t & \text{for Auger decay,} \\ P_{k3} = \Gamma_{ij}^{\mathrm{F}} \cdot \Delta t & \text{for fluorescence decay,} \end{cases}$$

where P_{k1}, P_{k2}, and P_{k3} are photoionization probability, Auger decay probability, and fluorescence decay probability, respectively. R_{ij} is the photoionization rate obtained by integrating the photoionization cross section with the photon frequency from Eq. (4). Γ_{ij}^{A} is Auger decay rate, and Γ_{ij}^{F} is fluorescence decay rate. Photoionization cross sections, Auger decay rates, and fluorescence decay rates are calculated by XATOM.

3. Take the random number of $[0,1]$ and choose to enter a channel or not. If the Kr atom enter a certain channel, the corresponding calculation of the electronic configuration is carried out.

4. Record the current time t and its electronic configuration, and repeat steps 2 and 3 until the maximum number of iterations is reached, or the Kr atom is completely ionized.

5. Repeat steps 2–4 and cycle for 10^6 times to obtain the patterns of population change with time.

6. Take the photon flux at different positions, get the population change data of each configuration corresponding to different photon flux, and record it into the database.

In this work, we ran 10^6 iterations to converge the results in a total of 8.19×10^4 configurations and 7.45×10^7 rate equations.

3. Results and discussion

3.1. Ionization kinetics of Kr in 17.50 keV

The time-dependent population obtained by the Monte–Carlo method is about spatial distribution. Therefore, we integrated the population change of each ion over space to obtain its time-dependent population change in Fig. 1,

$$n_i(t) = \int_0^1 n_i(t,r)\mathrm{d}r, \tag{6}$$

where $i = 1,2,3,\ldots,10$ is the ith ion whose population changes with time. We made a statistical analysis of the calculation results of the Monte–Carlo method and attained the time-dependent change of the population of ions. The theoretical calculation results at different positions are integrated over time and space, and the population is obtained from each charge state compared with the experimental values, which are shown in Fig. 2.

In comparison, our calculated value performed slightly worse in Kr^{7+}, and the other charge states with experimental values are better than the others.[27] When compared with the experimental values, there were some differences between the Kr^{1+}, Kr^{2+}, and Kr^{4+}. The differences are possibly due to the relatively few physical processes considered, such as single photon multi-ionization, double Auger decay, and resonant excitation to the parameter fitting,[20,28,29] which can provide better agreement to the experimental results.

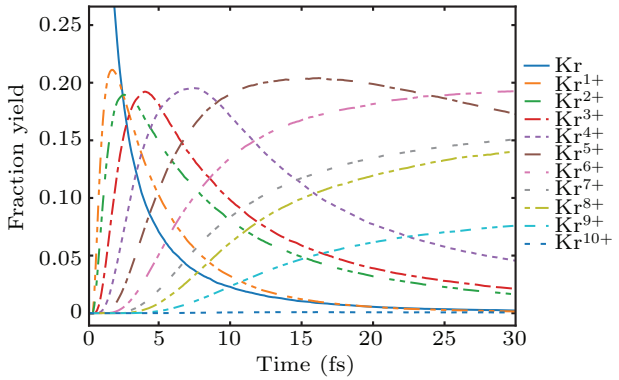


Fig. 1. The population of Kr ions varies with time. Pulse width is 30 fs.

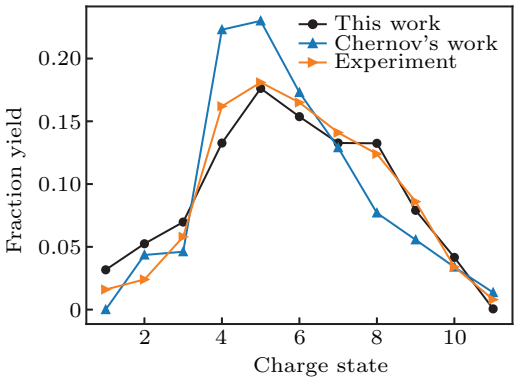


Fig. 2. Charge state distribution of Kr at 17.50 keV photon energy compared with experimental data[26] and another theoretical result.[27]

3.2. Selection of CIPEs

From Eq. (1), we present the relationship between total photoionization cross-section and photon energy. Figure 3 indicates that the photoionization cross-section decreases with increasing photon energy. The total photoionization cross-section changes rapidly at photon energies near 1.70 keV, 1.87 keV, and 14.00 keV. When the photon energy approaches the ionization energy of each orbital, there will be an increase in the total ionization cross-section. When the orbital electron is ionized, the corresponding orbital energy increases. When the photon energy is smaller than the elevated orbital energy, the corresponding orbital will no longer undergo single-photon ionization, resulting in the enhancement of light transparency. We define the value of CIPE in the range of ground state orbital energy and ionized orbital energy. The interval of CIPEs for 2p is 1.67–1.76 keV, 2s is 1.84–1.92 keV, and 1s is 14.02–14.43 keV. We take the CIPEs of three different orbitals as 1.75 keV, 1.90 keV, and 14.30 keV, respectively. In XFEL with high photon energy, this assumption is reasonable. We call an atom a hollow-like atom (HLA) that ionizes an electron from the electron orbital with the ground state's most significant non-inner photoionization cross-section. Table 1 shows a

comparison between hollow atoms and HLAs at three CIPEs and one experimental photon energy.

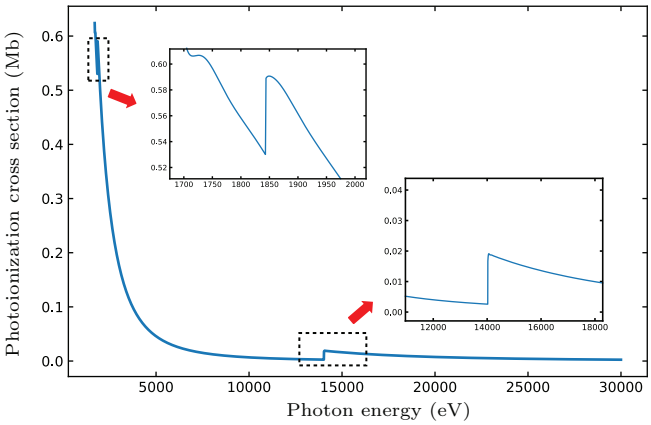


Fig. 3. Total photoionization cross-section of Kr to photon energy (1.70–30.00 keV).

Table 1. The total photoionization cross-section includes the sum of 8 photoionization cross-section channels of 1s–4p. The total rate includes 82 decay modes, 15 fluorescence decay rates and 67 Auger rates.

Photon energy (keV)	Configuration	Total ionization cross-section (Mb)	Total rates (a.u.)
1.75	$1s^22s^22p^6$	0.597	0.000
	$1s^22s^22p^5$	0.114	0.045
1.90	$1s^22s^22p^6$	0.561	0.000
	$1s^22s^12p^6$	0.510	0.031
14.30	$1s^22s^22p^6$	0.018	0.000
	$1s^12s^22p^6$	0.003	0.102
17.50	$1s^22s^22p^6$	0.011	0.000
	$1s^12s^22p^6$	0.006	0.102

At 1.75 keV, the total photoionization cross-section decreased from 0.597 Mb to 0.114 Mb before and after ionization, and 14.30 keV decreased from 0.018 Mb to 0.003 Mb. However, the total ionization cross-section at 1.90 keV did not decrease as expected because the ionization energy of 2s orbital was similar to that of 2p orbital. After ionization of 2s orbital electrons, the ionization energy of 2p orbital increased and approached 1.90 keV, resulting in the rise of the total ionization cross-section, which did not reach the expected attenuation value. 17.50 keV is a typical experimental parameter of photon energy from 1.7 keV to 30 keV. After the electron ionizes the inner orbital, the time and output of hollow atoms are less than the CIPE. It also shows that the saturable absorption of general photon energy is much lower than the CIPEs.

3.3. Temporal and spatial distribution of Kr hollow atoms

Hollow atoms are generated by ionizing the inner orbital energy close to the photon energy, which increases the decay rate and decreases the probability of atomic absorption of light. The generation of hollow atoms depends on time and photon flux.[11,12] However, in the actual process, we need to consider the distribution of spatial position as well. This paper assumes that the laser is a Gaussian beam, and the incident photon beam satisfies the Gaussian distribution in spatial position. Through different position parameters, three-dimensional images of spatial and temporal populations of hollow atoms of 1.75 keV, 1.90 keV, 14.30 keV, and 17.50 keV are obtained, which shows the effect on hollow atoms when the position parameters change.

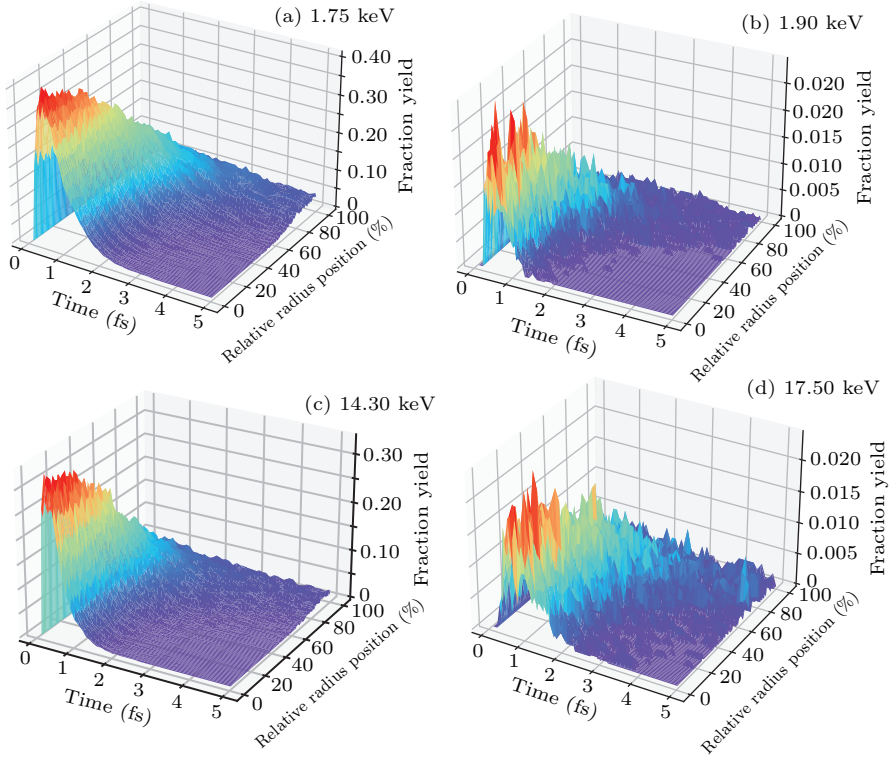


Fig. 4. Distribution diagram of hollow atoms and space. Time is from 0–5 fs, and position parameter is the relative radius position from 0–1 (100%).

From Fig. 4, we determined that 1.75 keV, 1.90 keV, 14.30 keV, and 17.50 keV reach the maximum average population of hollow atoms at 67%, 35%, 88%, and 26% of the radius from the center point. Due to the characteristics of Gaussian distribution, with the distance from the center, the photon flux decreases, the number of hollow atoms decreases, and the change of population slows down. The maximum values of three-dimensional images are 40.5%, 33.3%, 2.9%, and 2.4% showing that the hollow atom effect produced by the CIPE of 1s and 2p is higher than the CIPE of 17.50 keV and 2s, which is consistent with our prediction. By spatially integrating the image data, a more intuitive change of hollow atoms of Gaussian beams can be obtained.

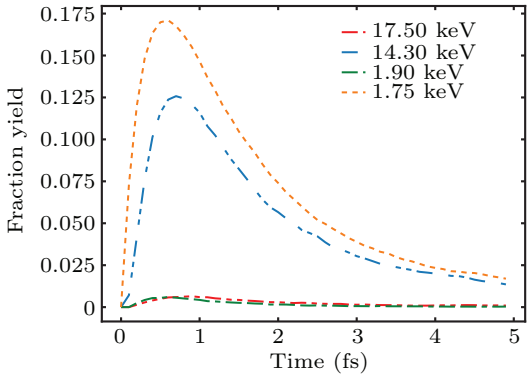


Fig. 5. Time-dependent population change of hollow(-like) atoms. 1.75 keV and 1.90 keV are HLAs.

Figure 5 shows that the populations of the two CIPEs of 1.75 keV and 14.30 keV are much higher than those of 1.90 keV and 17.50 keV photon energies, which reach the maximum at 0.6 fs and 0.7 fs. In the practical application of hollow atoms, the photon energy is the CIPE of the orbital with the largest angular momentum for a determined principal quantum number that can be selected to make the diffraction imaging of material structure detection clearer.

3.4. Ionization path diagram of Kr atom

In over 2×10^4 configurations, studying the comparison of main ionization paths under each photon energy can help better understand the direction of hollow atoms. Therefore, we count and plot the main ionization paths at the four specific photon energies.

Figure 6 demonstrates that under the photon energy of 1.75 keV and 1.90 keV, single-photon photoionization and Auger decay account for all channels of ion generation, and fluorescence decay does not occur. At 14.30 keV, the ion generation mainly depends on the ion generation mode of inner photoionization and Auger decay. At 17.50 keV, the inner photoionization cross-section decreases, and the generation of ions mainly depends on the ion generation mode of inner photoionization plus fluorescence decay. The photon energy is close to the orbital energy at low photon energy, and the photoionization cross-section is large. Thus there will be no fluorescence decay in the primary ionization process.

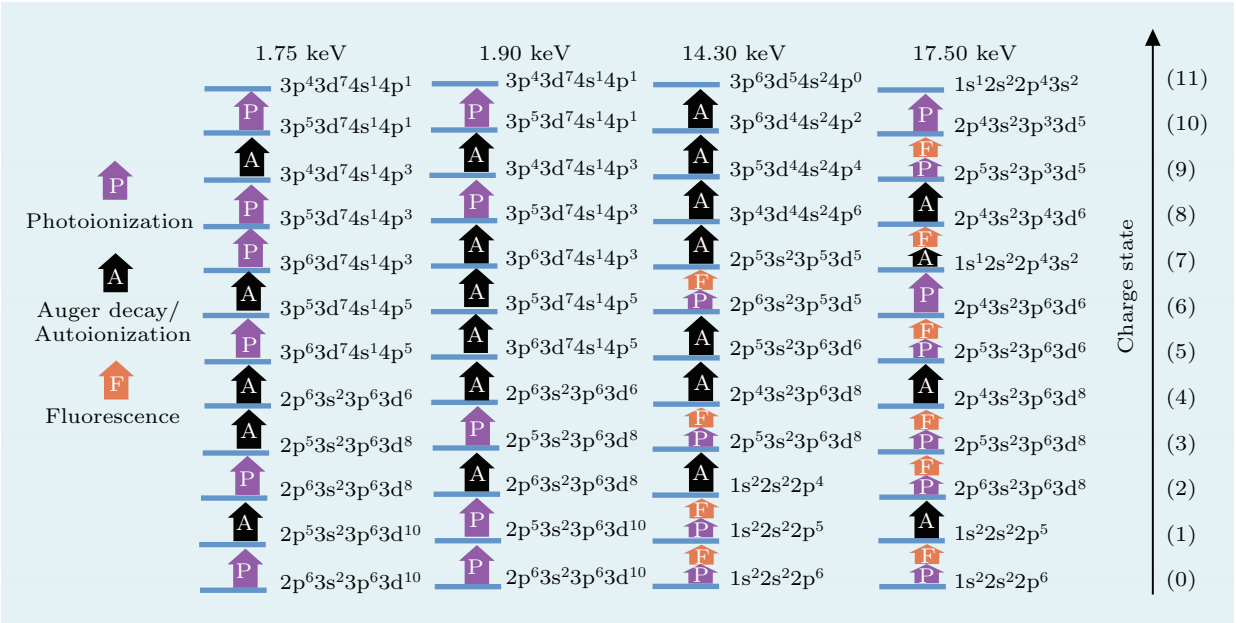


Fig. 6. Diagram of the dominant photon energy ionization path. Configurations not shown and not mentioned are full-occupied electron shells; configurations not shown but mentioned inherit the configuration from the previous step. The charge state is shown in parentheses on the right side. Fluorescence decay will affect whether the subsequent atoms choose ionization or Auger decay. Since fluorescence decay does not change the charge state, the arrows of photoionization and Auger decay that will change the charge state are placed together with fluorescence decay.

On the other hand, the photon energy is no longer close to the orbital energy at high photon energy, resulting in fluorescence decay after inner photoionization. For HLAs, 1.75 keV is no longer ionized after ionizing 2p orbital electrons, and the main channel is Auger decay; therefore, the population of HLAs is high. For 1.90 keV, after ionizing the 2s orbital elec-

trons, the photon energy is close to the 2p orbital energy. Then the 2p orbital ionization is mainly carried out, which is also the poor effect of producing hollow atoms in the CIPE. For hollow atoms, at 14.30 keV, because the photon energy is close to the inner orbital energy, and the ground state 1s photoionization cross-section and fluorescence decay ratio after ionization are higher than 17.50 keV at 14.30 keV, the hollow atom effect produced at 14.30 keV is more significant than 17.50 keV.

4. Conclusion

We used the Hartree–Fock–Slater model to calculate the total photoionization cross-section of the Kr atom in the range of 1.70–30.00 keV, calculated the ionization energy of each orbital of Kr, and finally determined three CIPEs of 1.75 keV, 1.90 keV, and 14.30 keV. We used the genetic algorithm to calibrate the parameters of the photon flux model in the results of calculating 17.50 keV photon energy Kr by the Monte–Carlo method and calculated the dynamical evolution of hollow atoms of 1.75 keV, 1.90 keV, 14.30 keV, and 17.50 keV. The conclusion indicates that the number of hollow atoms of 1.75 keV and 14.30 keV is much higher than that of the other two hollow atoms with ionization energy, which provides an idea for selecting photon energy in the subsequent application of hollow atoms. The main ionization paths of Kr atoms at photon energies of 1.75 keV, 1.90 keV, 14.30 keV, and 17.50 keV were studied. We suggest that the main ionization paths rarely produce fluorescence decay at low photon energy. In contrast, the generation of ions at high photon energy depends on the ionization mode of inner ionization and fluorescence decay, which provides an idea for understanding the ionization mode of high-Z atoms at different photon energies.

Acknowledgements

The authors would like to thank all the people who have been helping us in the theoretical calculation; particularly, our thanks go to Prof. Robin Santra, Dr. Yongjun Li, and Prof. Jianmin Yuan.

Project supported by the Fundamental Research Funds for the Central Universities (Grant No. 10822041A2038).

References

[1] Pellegrini C, Marinelli A and Reiche S 2016 *Rev. Mod. Phys.* **88** 015006
[2] Sobolev E, Zolotarev S, Giewekemeyer K, *et al.* 2020 *Commun. Phys.* **3** 97
[3] Lehmkühler F, Dallari F, Jain A, Sikorski M, Möller J, Frenzel L, Lokteva I, Mills G, Walther M, Sinn H, Schulz F, Dartsch M, Markmann V, Bean R, Kim Y, Vagovic P, Madsen A, Mancuso A P and Grübel G 2020 *Proc. Natl. Acad. Sci. USA* **117** 24110
[4] Pellegrini C 2012 *EPJ H* **37** 659
[5] Caleman C, Tîmneanu N, Martin A V, Jönsson H O, Aquila A, Barty A, Scott H A, White T A and Chapman H N 2015 *Opt. Express* **23** 1213
[6] Kobayashi A, Sekiguchi Y, Takayama Y, Oroguchi T and Nakasako M 2014 *Opt. Express* **22** 27892
[7] Ho P J, Kanter E P and Young L 2015 *Phys. Rev. A* **92** 063430
[8] Howells M, Beetz T, Chapman H, Cui C, Holton J, Jacobsen C, Kirz J, Lima E, Marchesini S, Miao H, Sayre D, Shapiro D, Spence J and Starodub D 2009 *J. Electron Spectros. Relat. Phenomena* **170** 4
[9] Doumy G, Roedig C, Son S K, *et al.* 2011 *Phys. Rev. Lett.* **106** 083002
[10] Nagler B, Zastrau U, Fäustlin R R, *et al.* 2009 *Nat. Phys.* **5** 693
[11] Deng P and Jiang G 2019 *Chin. Phys. B* **28** 063203
[12] Feng L and Jiang G 2017 *Acta Phys. Sin.* **66** 153201 (in Chinese)
[13] Yoneda H, Inubushi Y, Yabashi M, Katayama T, Ishikawa T, Ohashi H, Yumoto H, Yamauchi K, Mimura H and Kitamura H 2014 *Nat. Commun.* **5** 5080
[14] Son S K, Young L and Santra R 2011 *Phys. Rev. A* **83** 033402
[15] Decking W, Abeghyan S, Abramian P, *et al.* 2020 *Nat. Photon.* **14** 391
[16] Jia H, Huang S, Jiao Y, Li J, Liu K, Liu S, Liu W, Liu Z, Long T, Qin W and Zhao S 2022 *High Power Laser and Particle Beams* **34** 054001 (in Chinese)
[17] Murphy B F, Osipov T, Jurek Z, *et al.* 2014 *Nat. Comm.* **5** 4281
[18] Santra R 2009 *J. Phys. B* **42** 169801
[19] Toyota K, Jurek Z, Son S K, Fukuzawa H, Ueda K, Berrah N, Rudek B, Rolles D, Rudenko A and Santra R 2019 *J. Synchrotron Rad.* **26** 1017
[20] Li Y, Gao C, Zeng J and Yuan J 2022 *J. Phys. B* **55** 025002
[21] Gao C, Zeng J and Yuan J 2016 *J. Phys. B* **49** 044001
[22] Son S K and Santra R 2012 *Phys. Rev. A* **85** 063415
[23] Rudek B, Son S K, Foucar L, *et al.* 2012 *Nat. Photon.* **6** 858
[24] Wei B, Guo H, Ji Y, Hou S and Yin J 2020 *Chin. Phys. B* **29** 043701
[25] Maazouzi A E, Masrour R, Jabar A and Hamedoun M 2019 *Chin. Phys. B* **28** 057504
[26] Krause M O and Carlson T A 1967 *Phys. Rev.* **158** 18
[27] Chernov V E, Dorofeev D L, Elfimov S V, Zon B A, Gavrilov G E and Naryshkin Y G 2015 *Laser Phys. Lett.* **12** 036002
[28] Ho P J, Bostedt C, Schorb S and Young L 2014 *Phys. Rev. Lett.* **113** 253001
[29] Ding X, Wu C, Cao M, Zhang D, Zhang M, Xue Y, Yu D and Dong C 2020 *Chin. Phys. B* **29** 033101